Research Square

Preprints are preliminary reports that have not undergone peer review.
They should not be considered conclusive, used to inform clinical practice,
or referenced by the media as validated information.

Amyloid-Beta Deposition Patterns in Dementia with Lewy Bodies: Voxel-Wise Spatial Covariance Analysis and Associations with Core Clinical Features

Karolis Rozanas

karolis.rozanas@newcastle.ac.uk

Newcastle University

Sean Colloby
Newcastle University

Michael Firbank
Newcastle University

George Petrides
Newcastle upon Tyne Hospitals NHS Foundation Trust

Nicola Barnett
Newcastle University

Kirsty Olsen
Newcastle University

John-Paul Taylor
Newcastle University

Alan J. Thomas
Newcastle University

John T. O'Brien
University of Cambridge

Paul C. Donaghy
Newcastle University

Research Article

Keywords: Lewy body dementia, Amyloid, Florbetapir positron emission tomography, Spatial covariance analysis, Alzheimer disease

Posted Date: November 6th, 2026

DOI: https://doi.org/10.21203/rs.3.rs-11084372/v1

License: This work is licensed under a Creative Commons Attribution 4.0 International License.
Read Full License

Additional Declarations: Competing interest reported. Karolis Rozanas declares no competing interests. Sean Colloby declares no competing interests. Michael Firbank declares no competing interests. Paul C. Donaghy reports grants from Medical Research Council, Alzheimer's Society, Michael J Fox Foundation, GE Healthcare and Alzheimer's Research UK. George Petrides reports honoraria from GE Healthcare for delivering educational workshops on FP-CIT imaging, for FP-CIT clinical reporting, manuscript writing (not current manuscript) and for contributing to GE Healthcare led studies. He also receives fees for reporting PET CT scans from Alliance Medical Limited. Nicola Barnett declares no competing interests. Kirsty Olsen declares no competing interests. John-Paul Taylor has consulted for Takeda, Sumitomo, Eisai, CervoMed and Heptares-Sosei. He has received speaker fees from GE Healthcare and honoraria from the British Association of Psychopharmacology. He has received grants from Alzheimer's Society, Alzheimer's Research UK, the National Institute for Health and Care Research, the Lewy Body Society and the Medical Research Council. Alan J. Thomas reports grants from Alzheimer's Research UK, Alzheimer's Society, the Economic and Social Research Council, the Medical Research Council, the National Institute for Health and Care Research, the Lewy Body Society and GE Healthcare. John T. O'Brien reports grants from Alzheimer's Research UK, Alzheimer's Society, the Medical Research Council, the National Institute for Health and Care Research, the Lewy Body Society, Alliance Medical and Merck; personal fees from TauRx, Okwin, GE Healthcare, Novo-Nordisk; honoraria from the British Association of Psychopharmacology; and royalties from Taylor and Francis.

Abstract

Background

Amyloid co-pathology is common in Lewy body dementia, yet its spatial distribution and relationship to clinical heterogeneity remain unclear. Prior studies have focused on global burden or between-group comparisons rather than variation within Lewy body dementia.

Objectives

To determine whether Lewy body dementia exhibits a distinct spatial pattern of amyloid deposition relative to Alzheimer disease and controls, and to identify symptom-specific covariance patterns associated with its core features.

Methods

We performed voxel-wise principal component analysis of F-18 Florbetapir positron emission tomography scans from 77 participants (Lewy body dementia n = 35, Alzheimer disease n = 22, controls n = 20) to derive spatial covariance patterns. Spatial covariance analysis within the Lewy body dementia subgroup investigated patterns related to cognitive fluctuations, parkinsonism, rapid eye movement sleep behavior disorder and visual hallucinations.

Results

No distinct amyloid deposition pattern specific to Lewy body dementia was identified. Within the Lewy body dementia subgroup, covariance patterns were observed for cognitive fluctuations, characterized by left-lateralized frontal-temporal-striatal involvement; parkinsonism, demonstrating an anterior-posterior gradient; and rapid eye movement sleep behavior disorder, showing medial temporal involvement with frontal-parietal sparing. No pattern was identified for visual hallucinations.

Conclusions

Lewy body dementia does not exhibit a distinct amyloid deposition pattern, but regional variation in amyloid distribution may be associated with clinical heterogeneity. These findings suggest that cortical-network symptoms, particularly cognitive fluctuations, may relate to greater cortical amyloid co-pathology, whereas features linked to subcortical substrates, including parkinsonism and rapid eye movement sleep behavior disorder, may relate to cortical amyloid sparing.

Introduction

The diagnosis of dementia with Lewy bodies (DLB) is based primarily on core clinical features: cognitive fluctuations (CF), recurrent visual hallucinations (VH), rapid eye movement sleep behavior disorder (RBD) and parkinsonism, alongside diagnostic biomarkers (McKeith et al., 2017). However, DLB is clinically heterogeneous, potentially reflecting variation in α-synuclein distribution and co-pathologies, particularly amyloid-β (Aβ) deposition (Borghammer, 2021; Jellinger & Korczyn, 2018).

In vivo positron emission tomography (PET) imaging consistently shows that global Aβ burden in DLB is intermediate between healthy controls and Alzheimer disease (AD) (Yousaf et al., 2019; Tan et al., 2025). However, no DLB-specific spatial distribution has been identified (Yousaf et al., 2019). This may partly reflect reliance on global burden or region-of-interest analyses, which may lack sensitivity to detect distributed spatial covariance patterns (SCPs).

At a systems level, core DLB features map onto specific neural networks. Parkinsonism is associated with nigrostriatal degeneration (McGregor & Nelson, 2019), while RBD reflects dysfunction in brainstem circuits regulating rapid eye movement atonia (Elder et al., 2022; Joza et al., 2025). In contrast, CF and VH involve large-scale cortical attention and perceptual networks (O'Dowd et al., 2019; Matar et al., 2022; Shine et al., 2011; Zarkali et al., 2022).

In AD, Aβ deposition follows a characteristic neocortical progression (Thal et al., 2002). Concomitant AD pathology may therefore disproportionately influence DLB features associated with cortical networks, whereas its relative absence may be associated with phenotypes characterized by greater parkinsonism and RBD. This is broadly consistent with "brain-first" and "body-first" models of α-synuclein propagation, in which cortical regions are affected earlier in brain-first disease and brainstem structures earlier in body-first disease (Borghammer, 2021). Biomarker-defined DLB cases with AD co-pathology have been associated with increased cortical symptoms, particularly VH (Lemstra et al., 2017), whereas elevated cerebrospinal fluid tau has been linked to lower frequency of parkinsonism and RBD (Di Censo et al., 2019; Ferreira et al., 2020). However, findings are inconsistent (Jellinger, 2025), and prior work has largely relied on binary biomarker stratification rather than spatial modeling of Aβ distribution.

To address these issues, we applied voxel-wise spatial covariance analysis (SCA), a multivariate principal component analysis (PCA)-based approach that can identify distributed patterns of correlated tracer signal across brain regions. Similar methods have been applied to fluorine-18 fluorodeoxyglucose PET studies in dementia and Parkinson disease (Habeck et al., 2008; Ingram et al., 2022; Meles et al., 2020; Perovnik et al., 2022; Schindlbeck et al., 2020; Sigurdsson et al., 2022). We first performed pairwise SCA of florbetapir PET scans in DLB, AD and controls to derive diagnostic group-related amyloid patterns and then performed a DLB-specific analysis to examine symptom-associated patterns.

We hypothesized that DLB would show regional weighting patterns distinct from AD, potentially involving basal forebrain or occipital regions (Yousaf et al., 2019; Jellinger, 2025), and that cortical-dominant symptoms (CF and VH) would be associated with greater cortical amyloid signal, whereas subcortical-dominant symptoms (parkinsonism and RBD) would be associated with relative cortical sparing.

Methods

Study Design and Participants

This study was a secondary voxel-wise SCA reanalysis of ^{18}F-florbetapir PET data from the AMPLE cohort, a prospectively recruited study conducted between June 2013 and February 2016 in secondary care services in the North of England (Donaghy et al., 2018). Participants were aged ≥60 years. Dementia participants had probable DLB or AD according to contemporaneous consensus criteria (McKeith et al., 2005; McKhann et al., 2011). Although DLB participants were recruited before publication of the 2017 DLB Consortium criteria (McKeith et al., 2017), all fulfilled updated probable DLB criteria at retrospective verification. Diagnoses were determined independently by two experienced clinicians blinded to amyloid PET results.

Dementia participants required Mini-Mental State Examination (MMSE) ≥12 (Folstein et al., 1975). Controls were recruited from a research register or as partners of participants and required MMSE ≥26, with no clinical evidence of cognitive impairment. Exclusion criteria included major psychiatric illness, significant neurological disease, severe systemic illness, PET-CT contraindications, prior exposure to amyloid-targeting agents, or participation in investigational drug trials. Given the exploratory nature of this secondary analysis using an existing dataset, no a priori power calculation was performed.

Clinical Assessments

All participants underwent cognitive, neuropsychiatric and motor assessment as part of the original AMPLE protocol (Donaghy et al., 2018). Global cognition was assessed using Addenbrooke's Cognitive Examination-Revised (ACE-R) (Mioshi et al., 2006). Core DLB features were represented using Movement Disorder Society–Unified Parkinson's Disease Rating Scale Part III (MDS-UPDRS III) for parkinsonism (Goetz et al., 2008), Dementia Cognitive Fluctuation Scale (DCFS) for CF (Lee et al., 2014), and clinician consensus ratings for VH and RBD based on full clinical assessment and record review. VH and RBD were coded dichotomously because accurate severity scales were unavailable. Symptoms that had been present previously but were controlled at assessment, for example by treatment, were coded as present.

MRI Acquisition and Processing

Structural Magnetic Resonance Imaging (MRI) scans were acquired on a 3T Philips Achieva system using a 3D sagittal T1-weighted magnetization-prepared rapid gradient-echo sequence: repetition time 8.3 ms, echo time 4.6 ms, inversion time 1250 ms, flip angle 8°, and voxel size 1 × 1 × 1 mm (Donaghy et al., 2018). Images were processed using FreeSurfer (Fischl, 2012), with quality control by two blinded raters (Cohen's $\kappa = 0.92$) and manual correction where required. FreeSurfer-derived segmentations were used to generate the brain mask for PET SCA and to extract intracranial volume (ICV) and bilateral hippocampal volumes. Hippocampal volumes were normalized to ICV, and related analyses were restricted to participants with high-quality MRI data.

PET Acquisition and Processing

Participants underwent ^{18}F-florbetapir PET using a Siemens Biograph-40 PET-CT scanner (Siemens, Erlangen, Germany) after 370 MBq intravenous tracer injection (Donaghy et al., 2018). A 15-minute amyloid acquisition, comprising three 5-minute frames, was acquired 30–50 minutes post-injection. Images were reconstructed using iterative reconstruction with 4 iterations and 16 subsets, a 168 × 168 matrix, approximately 2.0 × 2.0 mm in-plane voxel size, 3-mm slice thickness, a 3-mm Gaussian post-reconstruction filter, and low-dose CT attenuation correction.

Mean PET images were spatially normalized to Montreal Neurological Institute (MNI) space before SCA. Statistical Parametric Mapping (SPM) was used for preprocessing (Ashburner & Friston, 2005). An MRI-derived brain mask defined the voxel space for analysis. Images were smoothed using a 10 mm full-width at half-maximum Gaussian kernel. To reduce intersubject global uptake effects, each subject's mean uptake within the analysis mask was removed from voxel intensity values before PCA. Participants without usable MRI volumetric data were retained in voxel-wise analyses because SCA did not require structural volumetric data.

Statistical and Spatial Covariance Analysis

Analyses were conducted using MATLAB R2017a with dedicated covariance analysis software. Additional processing was performed in Python and R where required.

Voxel-wise PCA was applied to spatially normalized and smoothed florbetapir images within the MRI-derived brain mask. Separate analyses were performed for controls versus AD, controls versus DLB, and AD versus DLB. For each comparison, participant scans were vectorized into a subjects-by-voxels matrix. Principal components (PCs) and corresponding subject scaling factors (SSFs) were generated for each analysis, with SSFs representing individual expression of each SCP.

To identify diagnostic group-related SCPs, SSFs were entered into linear regression models with diagnostic group as the dependent variable. Akaike's Information Criterion (AIC) was used to select the optimal combination of PCs balancing model fit and parsimony (Akaike, 1974). Selected PCs were linearly combined to produce a composite SCP for each diagnostic contrast, and individual pattern expression was quantified by projecting the composite pattern onto each participant's PET image.

A DLB-only SCA was then performed to identify symptom-associated tracer distribution patterns. DLB-specific PCs and SSFs were generated using the same approach. For each clinical variable, including DCFS score, MDS-UPDRS III score, RBD status and VH status, SSFs were entered as independent variables in linear regression models with the clinical measure as the dependent variable. AIC guided PC selection, and selected PCs were combined to generate symptom-specific SCPs.

Bootstrap resampling with 1000 iterations was used to assess pattern stability. In each iteration, PCA and regression-based model selection were repeated on resampled datasets. Voxel-wise Z-statistic

maps were calculated as the ratio of voxel weight to bootstrap-derived standard deviation (SD). A threshold of $|Z| \geq 1.64$ was used to identify voxels contributing reliably to each SCP.

Because component selection and pattern evaluation were performed within the same dataset, SSFs and associated model fits are reported as descriptive indices of pattern expression, and findings are interpreted as exploratory rather than confirmatory. Linear regression models examined associations between age, sex and DLB-specific SSF scores. Pearson correlation analysis examined associations between ICV-normalized bilateral hippocampal volume and SSF scores. SCPs were visualized using MRIcroGL, and regional contributions were localized using the AAL3 brain atlas.

Results

Participant Characteristics

The final sample comprised 77 participants: DLB (n = 35), AD (n = 22), and controls (n = 20) (Table 1). Groups were comparable in age and sex distribution. As expected, both dementia groups had lower ACE-R and MMSE scores than controls. Within the DLB group, RBD was present in 21/35 participants and VH in 22/35.

Spatial Covariance Analyses

Diagnostic Group Patterns

For controls versus AD, a composite image comprising PC_1, PC_2, PC_3, PC_4 and PC_{12} differentiated AD from controls, with higher SSF expression in AD (Figure 1a). The pattern associated with AD showed relatively higher posterior cortical and orbitofrontal florbetapir signal, with lower midline and medial temporal signal.

For controls versus DLB, a composite image comprising PC_1, PC_5 and PC_{12} distinguished DLB from controls, with higher SSF expression in DLB (Figure 1b). The pattern associated with DLB showed relatively higher florbetapir signal in right orbitofrontal and rectal cortices, with smaller temporal, cingulate, precuneus and frontal contributions.

For AD versus DLB, a composite image comprising PC_1, PC_4 and PC_8 separated DLB from AD, with higher SSF expression in DLB (Figure 1c). The pattern associated with DLB showed relatively higher fusiform and inferior temporal signal, with lower medial orbitofrontal, superior temporal and posterior cortical signal.

Symptom-Associated Patterns in DLB

A combination of PC_2, PC_5, PC_6 and PC_{10} was associated with increasing DCFS scores ($R^2 = 0.37$). The resulting SCP showed relatively higher florbetapir signal in the left putamen and frontal and temporal cortices, with lower right temporal signal, demonstrating a left-right asymmetric distribution (Figure 2).

The SCP associated with increasing MDS-UPDRS III scores comprised PC_3 only ($R^2 = 0.11$). This pattern demonstrated an anterior-posterior gradient, with relatively higher signal in anterior cortical, subcortical and medial temporal regions, and lower signal in posterior parietal and occipital cortices (Figure 3).

A combination of PC_1 and PC_4 was associated with positive RBD status ($R^2 = 0.28$). The pattern showed relatively higher signal in bilateral medial temporal regions and the caudate, with relative frontal-parietal sparing (Figure 4).

No SCP associated with VH positive status was identified following AIC-based model selection.

Relationship Between the RBD Pattern and Hippocampal Volume

Because increased medial temporal florbetapir signal in the RBD-associated pattern was unexpected, we explored whether this reflected relative medial temporal structural preservation. In DLB participants with high-quality MRI data (n = 29/35), RBD-associated SSF scores were positively correlated with ICV-normalized hippocampal volume ($r = 0.56$, $p = 0.002$).

Age and Sex Effects in DLB

Age and sex were associated with CF SSF scores only. CF SSF scores increased with age ($\beta = 1.483$, $p = 0.049$) and were higher in males than females ($\beta = 124.981$, $p = 0.049$; males: mean = 12.45, SD = 8.86; females: mean = 9.79, SD = 7.96). No associations were observed for parkinsonism, RBD or VH-related SSF scores.

Discussion

We combined whole-brain voxel-wise comparisons with within-DLB covariance modeling to examine spatial amyloid distribution and its relationship to clinical heterogeneity. We found no evidence of a DLB-specific amyloid topography, with substantial overlap between DLB and AD. Contrary to our hypothesis, DLB did not show greater basal forebrain or occipital florbetapir signal than AD. Within DLB, distinct symptom-associated covariance patterns were identified for CF, parkinsonism and RBD. These exploratory findings suggest that regional variation in florbetapir signal may relate to clinical heterogeneity, with CF linked to greater cortical amyloid co-pathology and parkinsonism and RBD linked to relative cortical amyloid sparing.

Absence of a DLB-Specific Amyloid Pattern

The lack of a DLB-specific amyloid topography is consistent with previous imaging studies showing that AD and DLB differ primarily in amyloid load rather than spatial deposition pattern (Yousaf et al., 2019). This supports the interpretation of amyloid pathology in DLB as coexisting Alzheimer-type pathology rather than a disease-specific amyloid pattern.

Cognitive Fluctuations: A Left-Lateralized Covariance Pattern

CF demonstrated the strongest association with an amyloid covariance pattern ($R^2 = 0.37$), characterized by a left-lateralized distribution involving frontal, temporal and striatal regions, and reduced loading in contralateral temporo-parietal and cerebellar areas. This spatial configuration overlaps with networks implicated in attention and arousal regulation, which are thought to underpin CF in DLB (Mengotti et al., 2020; O'Dowd et al., 2019; Matar et al., 2022). CF-related pattern expression increased with age and was higher in males. This contrasts with previous studies reporting broadly similar rates of cognitive fluctuations between sexes (Chiu et al., 2023). Given the marked male predominance of our sample, this finding may reflect residual confounding and should be interpreted cautiously.

Parkinsonism: An Anterior-Posterior Covariance Gradient

The covariance pattern associated with parkinsonism was modest ($R^2 = 0.11$) and demonstrated an anterior-posterior gradient, broadly inverse to the posterior-dominant florbetapir pattern observed in AD versus controls. This suggests that greater parkinsonism may be associated with relative absence of AD-like posterior cortical signal, consistent with evidence that parkinsonism is more prominent in DLB with lower concomitant Alzheimer-type pathology (Di Censo et al., 2019; Ferreira et al., 2020). The pattern also overlapped with motor and frontostriatal circuitry relevant to parkinsonism (McGregor & Nelson, 2019), although this should be interpreted cautiously given the exploratory analysis.

Rapid Eye Movement Sleep Behavior Disorder: Medial Temporal Signal and Structural Confounding

The RBD-associated covariance pattern ($R^2 = 0.28$) showed relatively increased medial temporal loading with reduced widespread cortical loading. Although medial temporal amyloid deposition is more typical of AD than DLB, the positive correlation between RBD-related SSF scores and hippocampal volume suggests that this signal may partly reflect structural preservation rather than greater amyloid burden. Together, these findings align with evidence that RBD is more frequent in DLB without comorbid AD pathology (Ferreira et al., 2020).

Visual Hallucinations: Null Findings

No amyloid covariance pattern was identified for VH. Although prior studies have linked AD co-pathology with increased hallucination frequency (Lemstra et al., 2017), our analysis was likely underpowered, and dichotomous coding may have reduced sensitivity. This null finding should therefore be interpreted cautiously.

Mixed Pathology and Clinical Heterogeneity

The CF- and parkinsonism-related covariance patterns align anatomically with attention-arousal and motor circuitry, respectively, supporting their neuroanatomical plausibility. The relative cortical involvement in CF, compared with cortical sparing in parkinsonism and RBD, is consistent with the hypothesis that AD-type amyloid co-pathology may preferentially modify symptoms associated with cortical networks. Conversely, parkinsonism and RBD may be more prominent in DLB phenotypes with less cortical amyloid co-pathology. This interpretation is conceptually consistent with brain-first and

body-first models of alpha-synuclein propagation (Borghammer, 2021), although the absence of tau and α-synuclein biomarkers precludes direct testing.

Strengths and Limitations

This study used a whole-brain voxel-wise framework rather than region-of-interest restriction, applying SCA to characterize between-group patterns and within-DLB symptom heterogeneity. FreeSurfer-derived gray matter masking was used to reduce nonspecific white matter binding and improve anatomical specificity.

Limitations include modest sample size, male predominance, cross-sectional design and dichotomous coding of VH and RBD, which likely reduced sensitivity to symptom-specific associations. Partial volume correction was not performed, and residual partial volume effects may have influenced regional signal estimates. Florbetapir PET is sensitive to amyloid but does not measure tau or alpha-synuclein, limiting interpretation of mixed proteinopathies. Finally, model selection and pattern evaluation were performed within the same dataset, increasing overfitting risk. The findings should therefore be considered exploratory pending replication in larger, longitudinal cohorts with multimodal biomarkers and continuous symptom measures.

Conclusions

Florbetapir signal distribution in DLB did not show a distinct spatial pattern compared with AD but was associated with core clinical features. CF was linked to greater cortical amyloid co-pathology, whereas parkinsonism and RBD were linked to relative cortical amyloid sparing. Larger longitudinal studies incorporating multimodal biomarkers are required to validate these exploratory findings.

Declarations

Acknowledgments

The authors thank the participants and families who took part in the original AMPLE study, as well as the clinical, research and imaging teams involved in recruitment, assessment and data acquisition.

Funding

This research was funded by the NIHR Newcastle Biomedical Research Centre (BRC) awarded to The Newcastle upon Tyne Hospitals NHS Foundation Trust, Faculty of Medical Sciences, Newcastle University and Cumbria, Northumberland, Tyne and Wear Foundation Trust.

Avid Radiopharmaceuticals, Inc., a wholly owned subsidiary of Eli Lilly and Company, enabled use of the 18F-florbetapir by providing tracer and funding scanner time, but was not involved in study design, data collection, data analysis, data interpretation, the writing of the report or the decision to submit the article for publication.

PCD is supported by the Medical Research Council [grant number MR/W000229/1].

JO'B is supported by the NIHR Cambridge Biomedical Research Centre and the Cambridge Centre for Parkinson's Plus Disorders. The UK Dementia Research Institute receives its funding from UK DRI, funded by the UK Medical Research Council, Alzheimer's Society and Alzheimer's Research UK.

Conflicts of interest/Competing interests

Karolis Rozanas declares no competing interests.

Sean Colloby declares no competing interests.

Michael Firbank declares no competing interests.

Paul C. Donaghy reports grants from Medical Research Council, Alzheimer's Society, Michael J Fox Foundation, GE Healthcare and Alzheimer's Research UK.

George Petrides reports honoraria from GE Healthcare for delivering educational workshops on FP-CIT imaging, for FP-CIT clinical reporting, manuscript writing (not current manuscript) and for contributing to GE Healthcare led studies. He also receives fees for reporting PET CT scans from Alliance Medical Limited.

Nicola Barnett declares no competing interests.

Kirsty Olsen declares no competing interests.

John-Paul Taylor has consulted for Takeda, Sumitomo, Eisai, CervoMed and Heptares-Sosei. He has received speaker fees from GE Healthcare and honoraria from the British Association of Psychopharmacology. He has received grants from Alzheimer's Society, Alzheimer's Research UK, the National Institute for Health and Care Research, the Lewy Body Society and the Medical Research Council.

Alan J. Thomas reports grants from Alzheimer's Research UK, Alzheimer's Society, the Economic and Social Research Council, the Medical Research Council, the National Institute for Health and Care Research, the Lewy Body Society and GE Healthcare.

John T. O'Brien reports grants from Alzheimer's Research UK, Alzheimer's Society, the Medical Research Council, the National Institute for Health and Care Research, the Lewy Body Society, Alliance Medical and Merck; personal fees from TauRx, Okwin, GE Healthcare, Novo-Nordisk; honoraria from the British Association of Psychopharmacology; and royalties from Taylor and Francis.

Ethics approval

The original AMPLE study was approved by the National Research Ethics Service Committee Northeast–Newcastle and North Tyneside 2 (REC reference: 13/NE/0064). The present study was a secondary

analysis of existing AMPLE study data.

Consent to participate

Written informed consent was obtained from participants with capacity. For participants lacking capacity, participation was authorized via consultee agreement in accordance with the Mental Capacity Act 2005.

Consent for publication

Not applicable.

Availability of data and material

The data analyzed in this study are available through Dementias Platform UK (https://www.dementiasplatform.uk/).

Code availability

The analysis code used for this study is not publicly available. Requests for access to relevant analysis scripts may be considered by the corresponding author and senior study investigators.

Author Contributions

Author contributions included conception and study design (PCD, SC, JPT, AJT and JTOB), data acquisition and original cohort organization (PCD, MF, GP, NB, KO, AJT and JTOB), image preparation (MF), statistical and image analysis (KR and SC), interpretation of results (KR, SC, MF, PCD, JPT, AJT and JTOB), drafting the manuscript (KR), critical revision for important intellectual content (all authors), and approval of the final version and agreement to be accountable for the integrity and accuracy of all aspects of the work (all authors).

References

1. Akaike, H. (1974). A new look at the statistical model identification. IEEE Transactions on Automatic Control, 19(6), 716–723. https://doi.org/10.1109/TAC.1974.1100705
2. Ashburner, J., & Friston, K. J. (2005). Unified segmentation. NeuroImage, 26(3), 839–851. https://doi.org/10.1016/j.neuroimage.2005.02.018
3. Borghammer, P. (2021). The α-synuclein origin and connectome model (SOC model) of Parkinson's disease: Explaining motor asymmetry, non-motor phenotypes, and cognitive decline. Journal of Parkinson's Disease, 11(2), 455–474. https://doi.org/10.3233/JPD-202481
4. Chiu, S. Y., Wyman-Chick, K. A., Ferman, T. J., Bayram, E., Holden, S. K., Choudhury, P., & Armstrong, M. J. (2023). Sex differences in dementia with Lewy bodies: Focused review of available evidence

and future directions. *Parkinsonism & Related Disorders, 107*, 105285. https://doi.org/10.1016/j.parkreldis.2023.105285

5. Di Censo, R., Abdelnour, C., Blanc, F., Bousiges, O., Lemstra, A. W., van Steenoven, I., Duyckaerts, C., & Hansson, O. (2019). CSF tau proteins correlate with an atypical clinical presentation in dementia with Lewy bodies. Journal of Neurology, Neurosurgery & Psychiatry, 91(1), 109–110. https://doi.org/10.1136/jnnp-2019-320980
6. Donaghy, P. C., Firbank, M. J., Thomas, A. J., Lloyd, J., Petrides, G., Barnett, N., Olsen, K., & O'Brien, J. T. (2018). Clinical and imaging correlates of amyloid deposition in dementia with Lewy bodies. Movement Disorders, 33(7), 1130–1138. https://doi.org/10.1002/mds.27403
7. Elder, G. J., Lazar, A. S., Alfonso-Miller, P., & Taylor, J.-P. (2022). Sleep disturbances in Lewy body dementia: A systematic review. International Journal of Geriatric Psychiatry, 37(10). https://doi.org/10.1002/gps.5814
8. Ferreira, D., Przybelski, S. A., Lesnick, T. G., Lemstra, A. W., Londos, E., Blanc, F., Nedelska, Z., Schwarz, C. G., Graff-Radford, J., Senjem, M. L., Fields, J. A., Knopman, D. S., Savica, R., Ferman, T. J., Graff-Radford, N. R., Lowe, V. J., Jack, C. R., Petersen, R. C., Mollenhauer, B., & Boeve, B. F. (2020). β-Amyloid and tau biomarkers and clinical phenotype in dementia with Lewy bodies. Neurology, 95(24), e3257–e3268. https://doi.org/10.1212/WNL.0000000000010943
9. Fischl, B. (2012). FreeSurfer. NeuroImage, 62(2), 774–781. https://doi.org/10.1016/j.neuroimage.2012.01.021
10. Folstein, M. F., Folstein, S. E., & McHugh, P. R. (1975). "Mini-mental state." A practical method for grading the cognitive state of patients for the clinician. Journal of Psychiatric Research, 12(3), 189–198. https://doi.org/10.1016/0022-3956(75)90026-6
11. Goetz, C. G., Tilley, B. C., Shaftman, S. R., Stebbins, G. T., Fahn, S., Martinez-Martin, P., Poewe, W., Sampaio, C., Stern, M. B., Dodel, R., Dubois, B., Holloway, R., Jankovic, J., Kulisevsky, J., Lang, A. E., Lees, A., Leurgans, S., LeWitt, P. A., Nyenhuis, D., … LaPelle, N. (2008). Movement Disorder Society-sponsored revision of the Unified Parkinson's Disease Rating Scale (MDS-UPDRS): Scale presentation and clinimetric testing results. Movement Disorders, 23(15), 2129–2170. https://doi.org/10.1002/mds.22340
12. Habeck, C., Foster, N. L., Perneczky, R., Kurz, A., Alexopoulos, P., Koeppe, R. A., Drzezga, A., & Stern, Y. (2008). Multivariate and univariate neuroimaging biomarkers of Alzheimer's disease. NeuroImage, 40(4), 1503–1515. https://doi.org/10.1016/j.neuroimage.2008.01.056
13. Ingram, M., Colloby, S. J., Firbank, M. J., Lloyd, J. J., O'Brien, J. T., & Taylor, J.-P. (2022). Spatial covariance analysis of FDG-PET and HMPAO-SPECT for the differential diagnosis of dementia with Lewy bodies and Alzheimer's disease. Psychiatry Research: Neuroimaging, 322, 111460. https://doi.org/10.1016/j.pscychresns.2022.111460
14. Jellinger, K. A. (2025). Concomitant pathologies and their impact on Parkinson disease: A narrative overview of current evidence. International Journal of Molecular Sciences, 26(7), 2942. https://doi.org/10.3390/ijms26072942

15. Jellinger, K. A., & Korczyn, A. D. (2018). Are dementia with Lewy bodies and Parkinson's disease dementia the same disease? BMC Medicine, 16(1), 34. https://doi.org/10.1186/s12916-018-1016-8
16. Joza, S., Camicioli, R., Ba, F., Ozzoude, M., McKeown, M. J., Wang, L., Stanley, O., Symes, M., Beaton, D., Binns, M., Kibreab, M., Scott, C., Ramirez, J., Masellis, M., Borrie, M., Bristol, L., Ducharme, S., Fisman, K., Freedman, M., Kumar, S., Lang, A., McLaughlin, P., Pollock, B., Rajji, T., Sahlas, D., Swartz, R., Finger, E., Fischer, C., Frank, A., Josviak, N., Tang-Wai, D., Black, S., Dowlatshahi, D., & ONDRI Investigators. (2025). Prodromal dementia with Lewy bodies in REM sleep behavior disorder: A multicenter study. Alzheimer's & Dementia, 20(1), 91–102. https://doi.org/10.1002/alz.13386
17. Lee, D. R., McKeith, I., Mosimann, U., Ghosh-Nyal, A., Grayson, L., Wilson, B., Aylward, B., Morris, M., Taylor, J.-P., & Thomas, A. (2014). The dementia cognitive fluctuation scale, a new psychometric test for clinicians to identify cognitive fluctuations in people with dementia. The American Journal of Geriatric Psychiatry, 22(9), 926–935. https://doi.org/10.1016/j.jagp.2013.01.072
18. Lemstra, A. W., de Beer, M. H., Teunissen, C. E., Schreuder, C., Scheltens, P., van der Flier, W. M., & Sikkes, S. A. M. (2017). Concomitant AD pathology affects clinical manifestation and survival in dementia with Lewy bodies. Journal of Neurology, Neurosurgery & Psychiatry, 88(2), 113–118. https://doi.org/10.1136/jnnp-2016-313775
19. Matar, E., Shine, J. M., Halliday, G. M., & Lewis, S. J. G. (2022). Dynamic network impairments underlie cognitive fluctuations in Lewy body dementia. npj Parkinson's Disease, 8(1), 16. https://doi.org/10.1038/s41531-022-00279-x
20. McGregor, M. M., & Nelson, A. B. (2019). Circuit mechanisms of Parkinson's disease. Neuron, 101(6), 1042–1056. https://doi.org/10.1016/j.neuron.2019.03.004
21. McKeith, I. G., Dickson, D. W., Lowe, J., Emre, M., O'Brien, J. T., Feldman, H., Cummings, J., Duda, J. E., Lippa, C., Perry, E. K., Aarsland, D., Arai, H., Ballard, C. G., Boeve, B., Burn, D. J., Costa, D., Del Ser, T., Dubois, B., Galasko, D., Gauthier, S., Goetz, C. G., Gomez-Tortosa, E., Halliday, G., Hansen, L. A., Hardy, J., Iwatsubo, T., Kalaria, R. N., Kaufer, D., Kenny, R. A., Korczyn, A., Kosaka, K., Lee, V. M.-Y., Lees, A., Litvan, I., Londos, E., Lopez, O. L., Minoshima, S., Mizuno, Y., Molina, J. A., Mukaetova-Ladinska, E. B., Pasquier, F., Perry, R. H., Schulz, J. B., Trojanowski, J. Q., & Yamada, M. (2005). Diagnosis and management of dementia with Lewy bodies: Third report of the DLB Consortium. Neurology, 65(12), 1863–1872. https://doi.org/10.1212/01.wnl.0000187889.17253.b1
22. McKeith, I. G., Boeve, B. F., Dickson, D. W., Halliday, G., Taylor, J.-P., Weintraub, D., Aarsland, D., Galvin, J., Attems, J., Ballard, C. G., Bayston, A., Beach, T. G., Blanc, F., Bohnen, N., Bonanni, L., Bras, J., Brundin, P., Burn, D., Chen-Plotkin, A., Duda, J. E., El-Agnaf, O., Feldman, H., Ferman, T. J., ffytche, D., Fujishiro, H., Galasko, D., Goldman, J. G., Gomperts, S. N., Graff-Radford, N. R., Honig, L. S., Iranzo, A., Kantarci, K., Kaufer, D., Kukull, W., Lee, V. M. Y., Leverenz, J. B., Lewis, S., Lippa, C., Lunde, A. M., Masellis, M., Masliah, E., McLean, P., Mollenhauer, B., Montine, T. J., Moreno, E., Mori, E., Murray, M., O'Brien, J. T., Orimo, S., Postuma, R. B., Ramaswamy, S., Ross, O. A., Salmon, D. P., Singleton, A., Taylor, A., Thomas, A., Tiraboschi, P., Toledo, J. B., Trojanowski, J. Q., Tsuang, D., Walker, Z., Yamada, M., & Kosaka, K. (2017). Diagnosis and management of dementia with Lewy bodies: Fourth

consensus report of the DLB Consortium. Neurology, 89(1), 88–100. https://doi.org/10.1212/WNL.0000000000004058

23. McKhann, G. M., Knopman, D. S., Chertkow, H., Hyman, B. T., Jack, C. R., Kawas, C. H., Klunk, W. E., Koroshetz, W. J., Manly, J. J., Mayeux, R., Mohs, R. C., Morris, J. C., Rossor, M. N., Scheltens, P., Carrillo, M. C., Thies, B., Weintraub, S., & Phelps, C. H. (2011). The diagnosis of dementia due to Alzheimer's disease: Recommendations from the National Institute on Aging-Alzheimer's Association workgroups. Alzheimer's & Dementia, 7(3), 263–269. https://doi.org/10.1016/j.jalz.2011.03.005
24. Meles, S. K., Renken, R. J., Pagani, M., Teune, L. K., Arnaldi, D., Morbelli, S., Nobili, F., van Laar, T., Obeso, J. A., Rodríguez-Oroz, M. C., & Leenders, K. L. (2020). Abnormal pattern of brain glucose metabolism in Parkinson's disease: Replication in three European cohorts. European Journal of Nuclear Medicine and Molecular Imaging, 47(2), 437–450. https://doi.org/10.1007/s00259-019-04570-7
25. Mengotti, P., Käsbauer, A.-S., Fink, G. R., & Vossel, S. (2020). Lateralization, functional specialization, and dysfunction of attentional networks. Cortex, 132, 206–222. https://doi.org/10.1016/j.cortex.2020.08.022
26. Mioshi, E., Dawson, K., Mitchell, J., Arnold, R., & Hodges, J. R. (2006). The Addenbrooke's Cognitive Examination Revised (ACE-R): A brief cognitive test battery for dementia screening. International Journal of Geriatric Psychiatry, 21(11), 1078–1085. https://doi.org/10.1002/gps.1610
27. O'Dowd, S., Schumacher, J., Burn, D. J., Bonanni, L., Onofrj, M., Thomas, A., Taylor, J.-P., & O'Brien, J. T. (2019). Fluctuating cognition in the Lewy body dementias. Brain, 142(11), 3338–3350. https://doi.org/10.1093/brain/awz235
28. Perovnik, M., Tomše, P., Jamšek, J., Tang, C., Eidelberg, D., & Trošt, M. (2022). Metabolic brain pattern in dementia with Lewy bodies: Relationship to Alzheimer's disease topography. NeuroImage: Clinical, 35, 103080. https://doi.org/10.1016/j.nicl.2022.103080
29. Schindlbeck, K. A., Lucas-Jiménez, O., Tang, C. C., Morbelli, S., Arnaldi, D., Pardini, M., Pagani, M., Ibarretxe-Bilbao, N., Ojeda, N., Nobili, F., & Eidelberg, D. (2020). Metabolic network abnormalities in drug-naïve Parkinson's disease. Movement Disorders, 35(4), 587–594. https://doi.org/10.1002/mds.27960
30. Shine, J. M., Halliday, G. M., Naismith, S. L., & Lewis, S. J. G. (2011). Visual misperceptions and hallucinations in Parkinson's disease: Dysfunction of attentional control networks? Movement Disorders, 26(12), 2154–2159. https://doi.org/10.1002/mds.23896
31. Sigurdsson, H. P., Yarnall, A. J., Galna, B., Lord, S., Alcock, L., Lawson, R. A., Colloby, S. J., Firbank, M. J., Taylor, J.-P., Pavese, N., Brooks, D. J., O'Brien, J. T., Burn, D. J., & Rochester, L. (2022). Gait-related metabolic covariance networks at rest in Parkinson's disease. Movement Disorders, 37(6), 1222–1234. https://doi.org/10.1002/mds.28977
32. Tan, J. H. K., Laurell, A. A. S., Sidhom, E., Rowe, J. B., & O'Brien, J. T. (2025). The effect of amyloid and tau co-pathology on disease progression in Lewy body dementia: A systematic review.

Parkinsonism & Related Disorders, 131, 107255. https://doi.org/10.1016/j.parkreldis.2024.107255

33. Thal, D. R., Rüb, U., Orantes, M., & Braak, H. (2002). Phases of Aβ-deposition in the human brain and its relevance for the development of AD. Neurology, 58(12), 1791–1800. https://doi.org/10.1212/WNL.58.12.1791
34. Yousaf, T., Dervenoulas, G., & Politis, M. (2019). Neuroimaging in Lewy body dementia. Journal of Neurology, 266(1), 1–26. https://doi.org/10.1007/s00415-018-8892-x
35. Zarkali, A., McColgan, P., Leyland, L. A., Lees, A. J., & Weil, R. S. (2022). Longitudinal thalamic white and grey matter changes associated with visual hallucinations in Parkinson's disease. Journal of Neurology, Neurosurgery & Psychiatry, 93(2), 169–179. https://doi.org/10.1136/jnnp-2021-326630

Table

Table 1. Clinical and Demographic Characteristics of the AMPLE Cohort

Variables	DLB (n=35)	AD (n=22)	Control (n=20)
Age (Mean ± SD)	75.9 ± 6.7	76.2 ± 6.6	76.4 ± 7.3
Gender (M/F)	30/5	17/5	16/4
ACE-R (Mean ± SD)	64 ± 15	61 ± 17	95 ± 3
MMSE (Mean ± SD)	21 ± 5	21 ± 5	29 ± 1
MDS-UPDRS Part III (Mean ± SD)	44 ± 18	16 ± 12	6 ± 4
DCFS (Mean ± SD)	11 ± 4	9 ± 4	–
RBD (+ / -)	21 / 14	–	–
VH (+ / -)	22 / 13	–	–

Values represent mean ± SD unless otherwise stated.

Abbreviations: ACE-R = Addenbrooke’s Cognitive Examination–Revised; MMSE = Mini-Mental State Examination; MDS-UPDRS Part III = Movement Disorder Society–Unified Parkinson’s Disease Rating Scale Part III; DCFS = Dementia Cognitive Fluctuation Scale; RBD = rapid eye movement sleep behavior disorder; VH = visual hallucinations; DLB = dementia with Lewy bodies; AD = Alzheimer disease; SD = standard deviation.

Figures

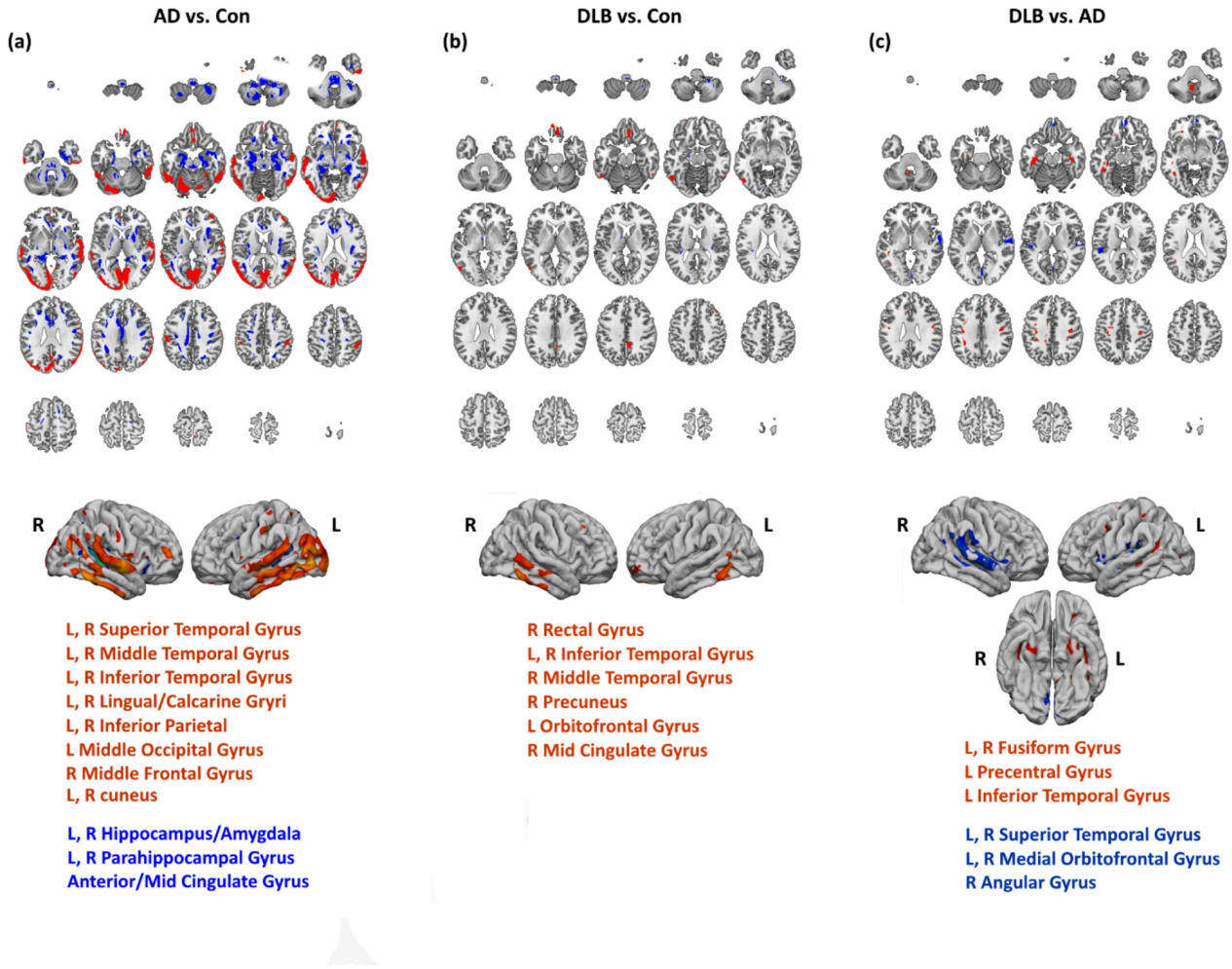


Figure 1

Between-group florbetapir spatial covariance patterns

Legend: Spatial covariance patterns (SCPs) derived from voxel-wise principal component analysis of ^{18}F-florbetapir PET images for diagnostic group comparisons: Controls vs AD (a), Controls vs DLB (b), and AD vs DLB (c). Patterns are displayed on axial slices and cortical surface-rendered MRI templates. Voxel-wise Z-score maps ($|Z| > 1.64$) illustrate regions contributing reliably to the reconstructed SCPs. Red regions indicate relatively higher florbetapir signal, whereas blue regions indicate relative lower florbetapir signal. Images are displayed in neurological convention (left is left).

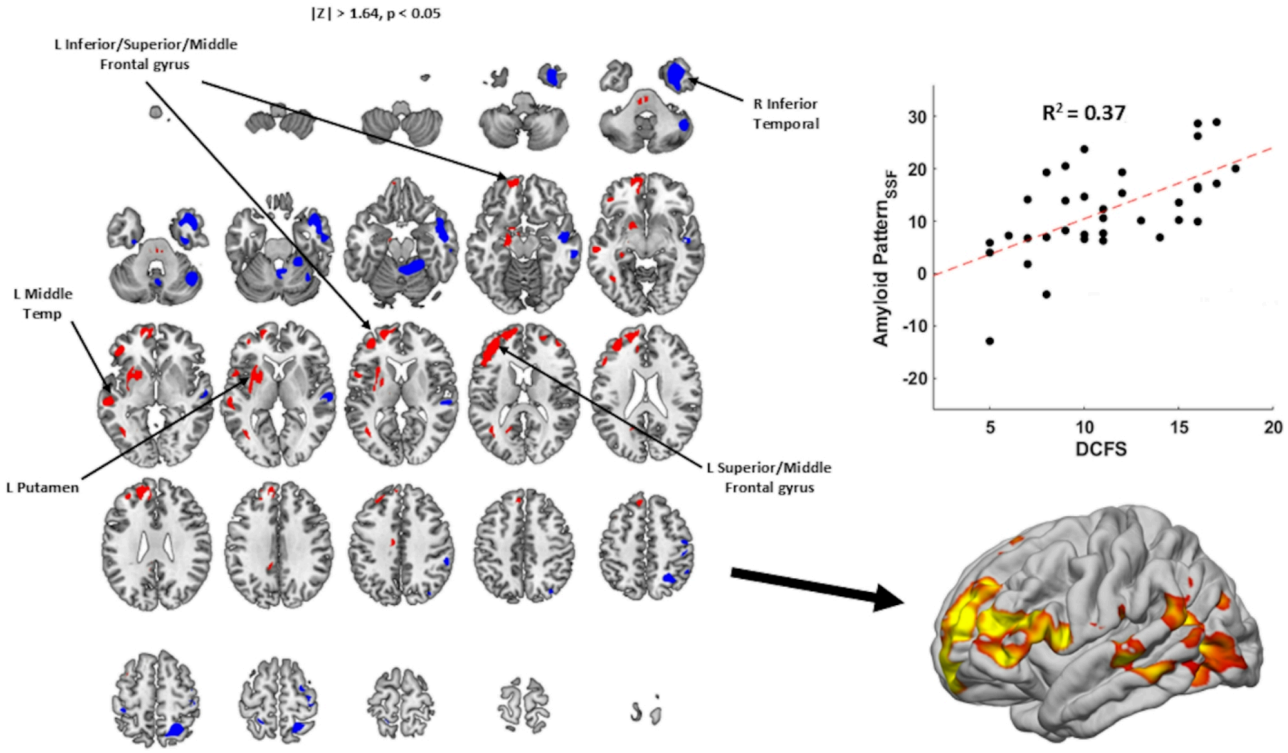


Figure 2

Florbetapir spatial covariance pattern associated with CF in DLB

Legend: Voxel-wise spatial covariance pattern (SCP) associated with Dementia Cognitive Fluctuation Scale (DCFS) scores in the DLB subgroup, derived from voxel-wise principal component analysis of ^{18}F-florbetapir PET images. Patterns are projected onto axial slices and cortical surface-rendered MRI templates. Voxel-wise Z-score maps (|Z| > 1.64) illustrate regions contributing reliably to the reconstructed SCP. Red areas indicate relative higher florbetapir signal with increasing DCFS scores, whereas blue areas indicate relative lower signal with increasing DCFS scores.The pattern demonstrates left-hemispheric predominance. The accompanying scatter plot illustrates the relationship between SCP expression scores (SSF) and DCFS scores.

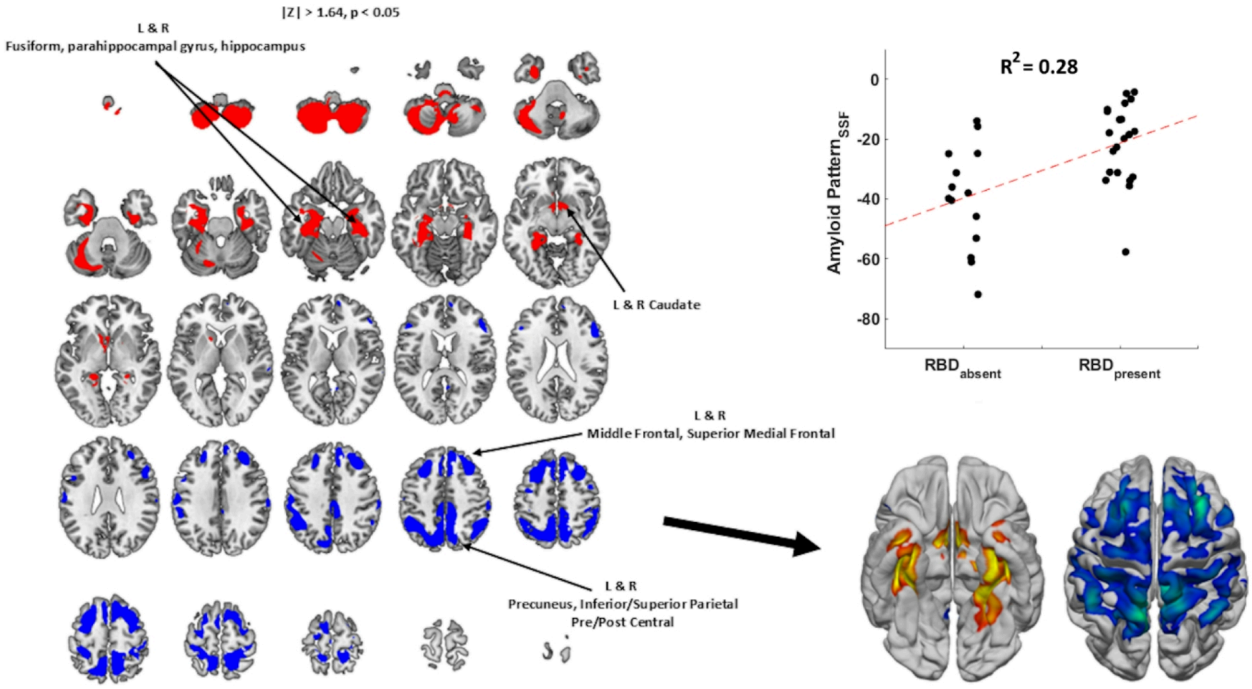


Figure 3

Florbetapir spatial covariance pattern associated with parkinsonism in DLB

Legend: Voxel-wise spatial covariance pattern (SCP) associated with MDS-UPDRS III scores in the DLB subgroup, derived from voxel-wise principal component analysis of ^{18}F-florbetapir PET images. Patterns are projected onto axial slices and cortical surface-rendered MRI templates. Voxel-wise Z-score maps (|Z| > 1.64) illustrate regions contributing reliably to the reconstructed SCP. Red regions indicate relative higher florbetapir signal with increasing MDS-UPDRS III scores, whereas blue regions indicate relative lower signal with increasing MDS-UPDRS III scores. The pattern demonstrates an anterior–posterior gradient. The accompanying scatter plot illustrates the relationship between SCP expression scores (SSF) and MDS-UPDRS III scores.

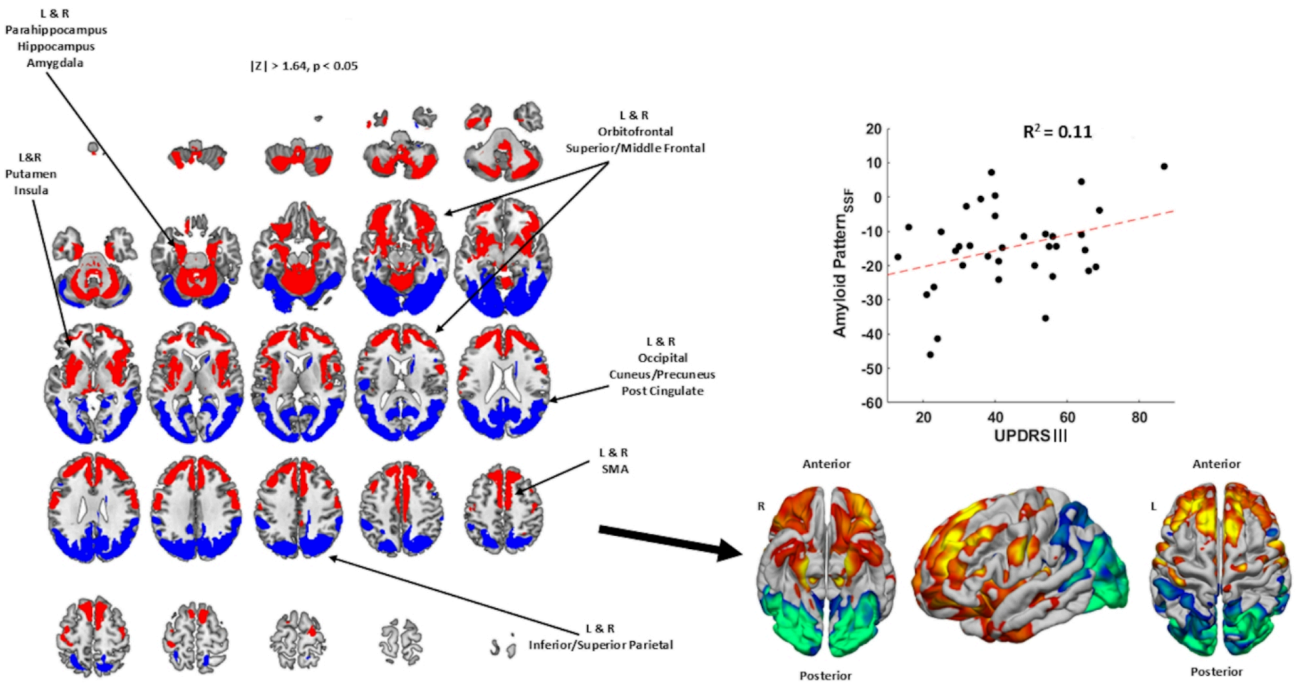


Figure 4

Florbetapir spatial covariance pattern associated with RBD in DLB

Legend: Voxel-wise spatial covariance pattern (SCP) associated with rapid eye movement sleep behavior disorder (RBD) status in the DLB subgroup, derived from voxel-wise principal component analysis of ^{18}F-florbetapir PET images. Patterns are projected onto axial slices and cortical surface-rendered MRI templates. Voxel-wise Z-score maps (|Z| > 1.64) illustrate regions contributing reliably to the reconstructed SCP. Red areas indicate relative higher florbetapir signal, whereas blue areas indicate relative lower signal in participants with RBD. The pattern demonstrates increased medial temporal and caudate signal with relative frontal–parietal sparing. The accompanying scatter plot illustrates the distribution of SCP expression scores (SSF) according to RBD status.